Chapter 36
Final Explosions and Collapse

We have seen that stars can evolve to the white dwarf stage through a sequence of consecutive hydrostatic states if they develop a degenerate core and have final masses less than the Chandrasekhar limit M_{Ch}. It is not well known, however, how much mass the stars can have initially (on the main sequence) in order to end this way. From what was discussed in Chap. 34, it seems that except for a very narrow mass range at the upper end, all stars that develop degenerate cores end as white dwarfs. The main uncertainty here is the total amount of mass lost by stellar winds.

Other stars certainly undergo explosions, ejecting a large part of their mass, if not disrupting completely. In the case where a neutron star is left as a remnant the core must have undergone a collapse, since it cannot reach the neutron-star stage by a hydrostatic sequence. Collapse and explosions are connected with supernova events, and although the theory and the numerical models are well developed and far advanced, not all questions concerning the different mechanisms have been answered, and not all different observed phenomena can be explained so far. The singular event of SN 1987A and the ongoing large-scale supernovae searches, which have returned hundreds of such objects throughout the universe, have led to a much better understanding of stellar explosions, but have also raised new questions. In this section we only discuss some basic effects which certainly play an important role in late phases of more massive stars, and that will probably remain to be an important part of full theories of supernovae.

Since we will not go into the details of the physics of collapse and explosion, and neither into the interesting question of explosive nucleosynthesis in supernovae, we refer the reader to the respective reviews on the subject, such as Hillebrandt and Niemeyer (2000; on supernovae of type I), Smartt (2009; on core collapse supernovae progenitors), Janka et al. (2007; on the theory of core collapse supernovae), Heger et al. (2003; on the fate of massive stars), and others.

R. Kippenhahn et al., *Stellar Structure and Evolution*, Astronomy and Astrophysics Library, DOI 10.1007/978-3-642-30304-3_36, © Springer-Verlag Berlin Heidelberg 2012

36.1 The Evolution of the CO-Core

After central helium burning, the further evolution depends critically on the question whether or not the CO-core becomes degenerate in the ensuing contraction phase. Clearly this will depend on the mass of the core. Since its contraction is practically independent of the envelope, the core can be considered as if it were a contracting gaseous sphere with zero surface pressure, as discussed in Chap. 28.

We first estimate the critical core mass that separates the case where the contraction leads to increasing temperatures from the case where degeneracy prevents further heating. For this purpose we replace the equation of state by an interpolation formula between different asymptotic behaviours. In the cores of evolved stars the molecular weight per electron is $\mu_e \approx 2$, while that per ion is $\mu_0 \geq 12$, and therefore the pressure of non-degenerate electrons ($\sim 1/\mu_e$) dominates the ion pressure ($\sim 1/\mu_0$). This holds even more so if the electrons are degenerate. For simplicity we here neglect radiation pressure, as well as the creation of electron–positron pairs, which can also lead to partial degeneracy at very high temperatures and low densities (see Sect. 36.3.5). We then approximate the equation of state by the simple form

$$P \approx P_e = \frac{\Re}{\mu_e}\varrho T + K_\gamma \left(\frac{\varrho}{\mu_e}\right)^\gamma . \tag{36.1}$$

In the second term the exponent γ is not a constant, allowing for non-relativistic and relativistic degeneracy. It varies from $\gamma = 5/3$ for $\varrho \ll 10^6\,\mathrm{g\,cm^{-3}}$ to $\gamma = 4/3$ for $\varrho \gg 10^6\,\mathrm{g\,cm^{-3}}$, while K_γ varies from the constant in (15.23) to that in (15.26).

The equation of hydrostatic equilibrium (2.4) yields as a rough estimate for the central values (which we denote by subscript 0):

$$P_0 \approx \frac{GM_c\bar{\varrho}}{R_c} = f G M_c^{2/3} \varrho_0^{4/3}. \tag{36.2}$$

Here we have used the fact that P_0 is almost given by the weight of the core material alone and $\bar{\varrho} = 3M_c/(4\pi R_c^3)$ is assumed to be proportional to ϱ_0. The dimensionless factor f, containing, for example, the ratio $\bar{\varrho}/\varrho_0$, is kept constant in this consideration. Using (36.1) for the centre and eliminating P_0 from (36.2) yields

$$\frac{\Re}{\mu_e} T_0 = f G M_c^{2/3} \varrho_0^{1/3} - K_\gamma \varrho_0^{\gamma-1} \mu_e^{-\gamma}. \tag{36.3}$$

On the right-hand side, the first term dominates in the non-degenerate case, while the two terms are about equal for high degeneracy.

For a given mass M_c, (36.3) gives an evolutionary track in the $\lg \varrho_0$–$\lg T_0$ plane in Fig. 36.1, similar to the tracks shown in Fig. 28.2. Starting with rather small ϱ_0 and $\gamma = 5/3$, the central temperature T_0 grows with ϱ_0 and has a maximum at $\varrho_{0\,\max}$, after which T_0 decreases again until $T_0 = 0$ is reached at a density of $8\varrho_{0\,\max}$.

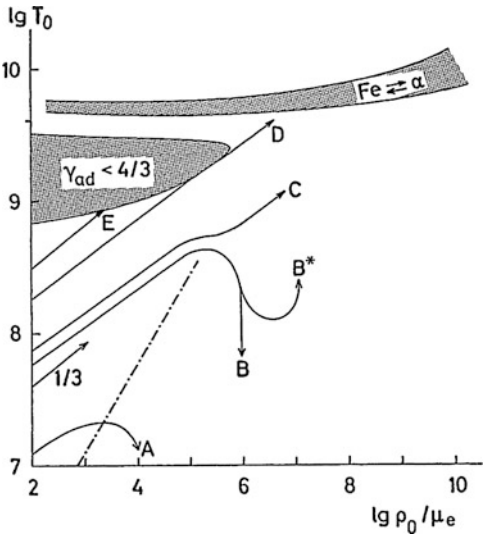

Fig. 36.1 Schematic evolution of the central values T_0 (in K) and ϱ_0 (in g cm^{-3}) for different core masses. The *dot-dashed line* corresponds to the left-hand part of the *dot-dashed line* in Figs. 28.1 and 28.2. Five evolutionary tracks are plotted which illustrate the different cases discussed in the text: A and B correspond to case 1. B^* illustrates case 2, where the core gains mass after it has become degenerate and undergoes a carbon flash. The curves C, D correspond to case 3, while curve E corresponds to case 4

The behaviour of these evolutionary tracks is the same as that discussed in Chap. 28, if there M is replaced by M_c (The way we have made our estimate here, keeping f constant during contraction, is equivalent to the assumption of homology there.). For example, in the non-degenerate case [first term on the right of (36.3) dominant], the slope of the tracks is 1/3 as indicated on the left-hand side of Fig. 36.1, and the tracks for different M_c are shifted at the same values of ϱ_0 like $T_0 \sim M_c^{2/3}$, in analogy to Sect. 28.1.

With sufficiently growing central density, relativistic degeneracy becomes important, and $\gamma \to 4/3$, $K_\gamma \to K_{4/3}$. If we now write $\gamma = 4/3 + \chi$ (where $\chi \to 0$ for $\varrho/\mu_e > 10^7$ g cm^{-3}), we can replace (36.3) by

$$\frac{\Re}{\mu_e} T_0 = \varrho_0^{1/3} \left(f G M_c^{2/3} - K_{(4/3+\chi)} \mu_e^{-(4/3+\chi)} \varrho_0^{\chi} \right) . \tag{36.4}$$

This shows that with increasing ϱ_0 the temperature T_0 does not become zero, but rises again $\sim \varrho^{1/3}$ if

$$M_c > M_{crit} = \left(\frac{K_{4/3}}{fG} \right)^{3/2} \mu_e^{-2} . \tag{36.5}$$

Obviously the critical value of M_c obtained in (36.5) is of the order of the Chandrasekhar mass M_{Ch} as in (19.29) and (19.30) [Note that a comparison of (36.1) with (19.3) shows that $K_{4/3} = K \mu_e^{4/3}$.]. In fact if $M_c = M_{crit}$ as defined here, then the core at zero temperature is fully relativistic, degenerate, and in hydrostatic equilibrium, which requires $M_c = M_{Ch}$.

We can therefore say that during contraction of a core with $M_c \lesssim M_{Ch}$ the central temperature reaches a maximum and afterwards decreases because of degeneracy,

while for $M_c \gtrsim M_{Ch}$, the temperature continues to increase, roughly proportionally to $\varrho_0^{1/3}$.

We consider next the maximum temperature an evolutionary track reaches for $M_c < M_{crit}$ in the non-relativistic regime. We simply set $\gamma = 5/3, K_\gamma = K_{5/3}$ in (36.3) and introduce M_{crit} from (36.5), obtaining

$$\Re T_0 = K_{4/3} \left(\frac{M_c}{M_{crit}}\right)^{2/3} \left(\frac{\varrho_0}{\mu_e}\right)^{1/3} - K_{5/3} \left(\frac{\varrho_0}{\mu_e}\right)^{2/3} . \tag{36.6}$$

This gives a maximum temperature T_{0max} for

$$\frac{\varrho_{0max}}{\mu_e} = \frac{1}{8} \left(\frac{K_{4/3}}{K_{5/3}}\right)^3 \left(\frac{M_c}{M_{crit}}\right)^2 \approx 2.38 \times 10^5 \text{g cm}^{-3} \left(\frac{M_c}{M_{crit}}\right)^2 , \tag{36.7}$$

with the value

$$T_{0max} = \frac{1}{4\Re} \frac{K_{4/3}^2}{K_{5/3}} \left(\frac{M_c}{M_{crit}}\right)^{4/3} \approx 0.5 \times 10^9 \text{K} \left(\frac{M_c}{M_{crit}}\right)^{4/3} . \tag{36.8}$$

(Note that $K_{4/3}$ and $K_{5/3}$ have different dimensions.) For cores with $M_c \lesssim M_{crit}$, therefore, T_0 cannot exceed $\approx 0.5 \times 10^9$ K. This is in rough agreement with the "summit" of the dotted line in Fig. 28.1.

The events in the following stages depend sensitively on details of the material functions, the initial models, and the numerical calculations. These factors can decide, for example, whether core collapse is followed by an explosion, whether a remnant is left, etc. In view of the uncertainties involved and the many complications which can occur, it is not surprising that the present picture is not too clear (see Heger et al. 2003 for an overview of possibilities). Nevertheless we will tentatively classify the different evolutionary scenarios according to the core mass M_c after helium burning. As can be seen, for example, from (36.3), the tracks for lower mass are below those for higher mass. We distinguish four cases, each of which is represented by one or more schematic evolutionary tracks in Fig. 36.1.

Case 1. If $M_c < M_{crit} \approx M_{Ch}$, and if the envelope is not massive enough (due either to the original mass or to mass loss), so that M_c cannot approach M_{Ch} during the shell burning phase, T_0 first grows in the non-degenerate regime until a maximum is reached. Then the core becomes degenerate, starts to cool, and the star must become a white dwarf. This is most likely the fate for most intermediate mass stars, which evolve as single stars (Chap. 34; Fig. 34.7). Only if a star is a member of a binary system and accretes sufficient mass at certain rates carbon can finally be ignited in a flash. A very popular scenario is the *double-degenerate* one, in which a CO-WD and a He-WD in a binary system merge due to the loss of angular momentum by gravitational radiation. It would explain how the CO core would reach M_{Ch} and why the spectrum would be devoid of hydrogen lines (the definition of type I supernovae). From the shell in which the flash occurs, a helium detonation

wave (see Sect. 36.2.4) starts, moving both out- and inwards (This is in fact a simplified one-dimensional picture; in reality the flash occurs at a certain location, and the front travels in all directions and even around the star.). When it arrives near the centre, carbon will be ignited and a second (carbon) detonation front moves outwards, too. In this double-detonation model the star will finally be disrupted (for a summary see, for instance, Hillebrandt and Niemeyer 2000). Alternatively, in the *single degenerate scenario*, the CO-WD accretes matter from a non-degenerate companion. This could be a main-sequence star or a giant, for example, on the RGB. If the mass transfer rate is favourable, the accreted matter is burnt hydrostatically and the core grows in mass up to $M_{\rm Ch}$. Again, the envelope is hydrogen free and the spectrum would classify the supernova as of type I. In this scenario the previous loss of matter in the pre-WD evolution is effectively reversed. A third possibility is that explosions in the accreted helium layers shock the CO-core sufficiently to trigger a nuclear runaway, although the core has not reached the Chandrasekhar mass. These are the *Sub-Chandrasekhar models*. In all three cases the explosion of the star is due to a thermonuclear runaway resulting from the carbon flash. These are the type Ia supernovae. We will discuss basic facts of the carbon flash briefly in Sect. 36.2.

Case 2. If initially $M_{\rm c} < M_{\rm crit}$, but if the remaining envelope is sufficiently massive, so that because of shell burning, $M_{\rm c}$ can grow to $M_{\rm Ch}$, the core becomes degenerate and cools after having reached a maximum temperature. But ϱ_0 increases with $M_{\rm c}$, and finally carbon burning begins (e.g. by pycnonuclear reactions; compare with Sect. 35.2). It starts in a highly degenerate state and is therefore explosive. This carbon flash can occur in stars that have started on the main sequence in the range $4 \lesssim M/M_\odot < 8$, if their mass loss has not been too strong. However, as we have mentioned before, this seems to be unlikely, although it cannot be excluded completely, for example, in the case of extremely metal-poor or metal-free stars (so-called Population III or *First Stars*), where mass loss may be significantly lower than in stars of solar metallicity (Chap. 9). Since the spectrum in such an event would contain hydrogen lines, as is the definition for type II supernovae, but the explosion mechanism is that of a thermonuclear runaway, typical for type Ia supernovae, such events are called supernovae of type 1.5. Whether they exist remains unclear.

Case 3. If $M_{\rm crit} < M_{\rm c} \lesssim 40 M_\odot$, the evolutionary track misses the non-relativistic region of degeneracy. The core heats up, reaching successively higher nuclear fusion phases. In a small mass range above the minimum mass to start carbon burning (this critical mass is usually refered to as $M_{\rm up}$; see Fig. 34.10), electron captures by Mg, Na, and Ne reduce the pressure and a central collapse ensues. This is the fate of some of the super-AGB stars of Sect. 34.8, if the mass of the resulting NeO-core is initially below $1.37 M_\odot$ to avoid Ne ignition, but reaches this critical value due to shell burning. This will be discussed further in Sect. 36.3.4. The corresponding CO-core mass limit is of order $2-4 M_\odot$. For $M_{\rm c} \gtrsim 4 M_\odot$, photodisintegration of Ne and Mg nuclei brings $\gamma_{\rm ad}$ below $4/3$ and triggers a collapse. Both types of collapse may lead to neutron-star formation and to the ejection of the envelope, the latter mechanism also to black holes as the stellar remnants. It is assumed to cause the standard type II supernovae, and will be introduced in Sect. 36.3.

Case 4. : If $M_c \gtrsim 40 M_\odot$, the cores also reach the carbon burning in a non-degenerate state as in Case 3. This mass limit is, as always, metallicity dependent, and corresponds to helium-core mass of $\approx 65 M_\odot$ and an initial mass of $\approx 140 M_\odot$. After carbon burning the evolutionary tracks in Fig. 36.1 cross the region of pair creation, which also reduces γ_{ad}. If $\gamma_{ad} < 4/3$ in an appreciable fraction of the core, say, within 40 % of its mass, then the core collapses adiabatically until the temperature of oxygen burning is reached. This may stop the collapse and make the star explode; if not, the collapse would lead into the region of instability because of photodisintegration, and the events would be as in Case 3. We will discuss this in Sect. 36.3.5. The remnants of stars in this mass range will be neutron stars (for lower masses), black holes by fallback on the proto-neutron star, or black holes by direct formation. Pair-instability supernovae, a subclass of type II core collapse supernovae, leave no remnant at all.

36.2 Carbon Ignition in Degenerate Cores

Consider stars starting with masses in the range $4 \lesssim M/M_\odot \lesssim 8$ and assume that they have almost no mass loss. After helium burning, they will form a CO-core that is degenerate, and in the subsequent evolution, M_c grows owing to shell burning until it comes close to M_{Ch}. During this phase the central density increases with increasing M_c (similar to a sequence of white dwarfs with increasing mass). The energy released in the core during this contraction is transported by electron conduction in the direction of the centre, where the temperature is smaller and neutrino losses (see Sect. 18.7) carry away the energy. The increase of the central density or of the temperature at the place of its maximum finally ignites carbon burning.

36.2.1 The Carbon Flash

The ignition of carbon in degenerate CO-cores of mass $M_c \approx M_{Ch}$ has already been discussed in Sect. 35.2. As described there, the ignition of carbon may occur in the centre or in the shell of maximum temperature. The general properties of the flash are the same in both cases. We discuss here the central ignition in the case of strong degeneracy, but recall that most likely only stars above $8 M_\odot$ will reach carbon ignition and this will happen off-centre at very modest degeneracy. The carbon flash under such circumstances is described in the literature about super-AGB stars, for example, by García-Berro and Iben (1994).

In Fig. 36.2 the lg ϱ_0-lg T_0 plane is shown again with an evolutionary path of the centre. The stability behaviour of the degenerate core depends critically on the question whether the energy balance is dominated by neutrino losses ($\varepsilon_{CC} - \varepsilon_\nu < 0$: stable) or by carbon burning ($\varepsilon_{CC} - \varepsilon_\nu > 0$: unstable).

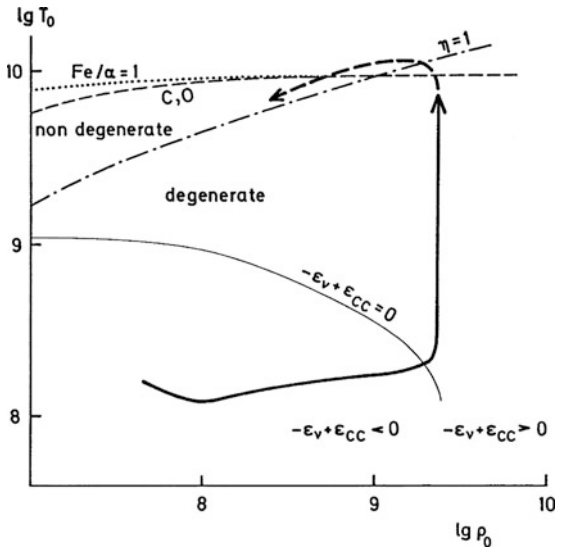

Fig. 36.2 Schematic evolution of the central region during and after the carbon flash (*heavy*). It corresponds to the evolution of type B^* in Fig. 36.1. The flash starts when the central density ϱ_0 (in $\mathrm{g\,cm^{-3}}$) or the central temperature T_0 (in K) is so high that the neutrino losses do not overcome the energy generation by carbon burning. The temperature then rises almost at constant density until degeneracy is removed. The *dot-dashed line* labelled $\eta = 1$ indicates where the gas pressure is twice the (degenerate) pressure at temperature zero; it roughly separates the regions of degeneracy and non-degeneracy. The *broken line* labelled C, O gives the temperature reached if all the energy released by carbon burning is used to increase the internal energy. The *dotted line* labelled Fe/α = 1 shows the points for which statistical equilibrium gives equal abundances of iron and helium

The borderline $\varepsilon_{\mathrm{CC}} - \varepsilon_\nu = 0$ bends down at a few $10^9\,\mathrm{g\,cm^{-3}}$, since $\varepsilon_{\mathrm{cc}}$ here increases mainly with increasing density (pycnonuclear reactions, see Sect. 18.4). Numerical calculations indicate that CO-cores reach the critical border $\varepsilon_{\mathrm{CC}} - \varepsilon_\nu = 0$ between stability and instability at a density of $2 \times 10^9\,\mathrm{g\,cm^{-3}}$.

The slightest increase in temperature now makes $\varepsilon_{\mathrm{CC}} - \varepsilon_\nu > 0$. Because of degeneracy the pressure does not increase and there is no consumption of energy through expansion. Therefore the temperature rises even more: a violent flash occurs. As in the case of the helium flash (see Sect. 33.4) the involved matter heats up at constant density until degeneracy is removed. Then it expands.

36.2.2 Nuclear Statistical Equilibrium

How violent the carbon flash can become is seen from a simple estimate. In a mixture of equal parts of C and O the carbon burning can release 2.5×10^{17} erg/g and

the subsequent oxygen burning twice this amount. If all this energy is used to heat the material, it can reach the temperatures indicated by the dashed line labelled C, O in Fig. 36.2. This line is somewhat curved since the specific heat depends slightly on the density. At these temperatures of nearly 10^{10} K the energy of the photons exceeds the binding energy of the nuclei, which are thus disintegrated. Photodisintegration, for example, of Ne nuclei

$$^{20}\mathrm{Ne} + \gamma \rightarrow ^{16}\mathrm{O} + \alpha, \tag{36.9}$$

was discussed in Sect. 18.5.3. The inverse reaction of (36.9) can also occur, and the photon generated by this process can disintegrate another Ne nucleus. The processes are very similar to ionization and recombination of atoms. In nuclear statistical equilibrium (*NSE*) the abundances of O, Ne, and α particles can be derived from a set of equations similar to the Saha equation (14.11):

$$\frac{n_{\mathrm{O}} n_\alpha}{n_{\mathrm{Ne}}} = \frac{1}{h^3}\left(\frac{2\pi m_{\mathrm{O}} m_\alpha kT}{m_{\mathrm{Ne}}}\right)^{3/2} \frac{G_{\mathrm{O}} G\alpha}{G_{\mathrm{Ne}}}\, \mathrm{e}^{-Q/kT}, \tag{36.10}$$

where G_{O}, G_α, and G_{Ne} are the statistical weights, while Q is the difference of binding energies

$$Q = (m_{\mathrm{O}} + m_\alpha - m_{\mathrm{Ne}})c^2. \tag{36.11}$$

In addition to (36.10) there are two other conditions, one of which relates the particle numbers to the density, the other one describing the initial composition, since (36.9) and its inverse cannot change $n_{\mathrm{O}} - n_\alpha$. Of course, one cannot consider a single reaction only, but has to take into account all reactions that can take place simultaneously. For example, α particles generated by (36.9) can also be captured by ^{12}C or ^{20}Ne (The problem is similar when ionization of different elements takes place simultaneously. They are not independent of each other, since all of them produce electrons which influence all recombination rates.).

If the temperatures are sufficiently high, many nuclei are disintegrated by photons and their fragments react again. The abundances of the different elements are then determined by a set of "Saha formulae" of the type (36.10). The nucleus $^{56}_{26}$Fe as the most stable one plays a crucial role in this statistical equilibrium. It can be disintegrated by photons into α particles and neutrons:

$$\gamma + ^{56}_{26}\mathrm{Fe} \rightleftarrows 13\alpha + 4\mathrm{n}. \tag{36.12}$$

In order to determine the ratio n_{Fe}/n_a we consider quite general reactions of the type

$$\gamma + (Z, A) \rightleftarrows (Z - 2, A - 4) + \alpha, \tag{36.13}$$

$$\gamma + (Z, A) \rightleftarrows (Z, A - 1) + \mathrm{n}. \tag{36.14}$$

We start with the nucleus $(26, 56) = {}^{56}\mathrm{Fe}$ and consider 13 reactions of type (36.13) and four of type (36.14). Then the abundance ratios are all given by equations like (36.10), and they can be combined to

$$\frac{n_\alpha^{13} n_\mathrm{n}^4}{n_\mathrm{Fe}} = \frac{G_\alpha^{13} G_\mathrm{n}^4}{G_\mathrm{Fe}} \left(\frac{2\pi kT}{h^2}\right)^{24} \left(\frac{m_\alpha^{13} m_\mathrm{n}^4}{m_\mathrm{Fe}}\right)^{3/2} \mathrm{e}^{-Q/kT}, \tag{36.15}$$

with

$$Q = (13m_\alpha + 4m_\mathrm{n} - m_\mathrm{Fe})c^2. \tag{36.16}$$

If one assumes that the numbers of protons to neutrons (independently of whether they are free or in nuclei) have a ratio $n_\mathrm{p}/n_\mathrm{n} = 13/15$, as it is in the nucleus ${}^{56}\mathrm{Fe}$, then

$$n_\mathrm{n} = \frac{4}{13} n_\alpha. \tag{36.17}$$

This, for instance, would be approximately the case in a mixture in which ${}^{56}\mathrm{Fe}$ is by far the most abundant heavy nucleus and its disintegration yields almost all neutrons and α particles. Then the left-hand side of (36.15) can be replaced by

$$\left(\frac{4}{13}\right)^4 \frac{n_\alpha^{17}}{n_\mathrm{Fe}}. \tag{36.18}$$

Ignoring the binding energies, we can write the density as

$$\varrho = (56n_\mathrm{Fe} + 4n_\alpha + n_\mathrm{n})m_\mathrm{u}, \tag{36.19}$$

where m_u is the atomic mass unit. For given values of ϱ, T, and the ratio n_n/n_α [corresponding to (36.17)] with (36.15), (36.18) and (36.19) we have two equations for n_Fe and n_α.

Suppose again that the ratio of protons to neutrons per unit volume, normally called $\bar{Z}/\bar{N}$, is 13/15. Then equilibrium demands that all matter goes into ${}^{56}\mathrm{Fe}$ (the nucleus of the highest binding energy per nucleon) for temperatures that are not too high, and into ${}^4\mathrm{He}$ for high temperatures (see Fig. 36.3a). However, if we assume $\bar{Z}/\bar{N} = 1$, then for the former temperatures ${}^{56}_{28}\mathrm{Ni}$ is the dominant nucleus, since it has the highest binding energy per nucleon of all nuclei with $Z = N$. With increasing temperature the equilibrium shifts from ${}^{56}\mathrm{Ni}$ to ^{54} Fe+2p and finally to 14 ${}^4\mathrm{He}$. For very high temperatures it may even shift to the basic constituents, protons and neutrons (see Fig. 36.3b).

The value $\bar{Z}/\bar{N}$ at the occurrence of photodisintegration depends on the weak interaction processes (β decays) during the nuclear history of the stellar matter. In any case, in equilibrium at moderate temperatures, one expects nuclei of the iron group, which with increasing temperature disintegrate to α particles and at temperatures around 10^{10} K, which can also be reached in exploding cores, even to protons and neutrons. In this case, (36.12)–(36.19) would have to be written for ${}^{56}\mathrm{Fe}$, n, and p.

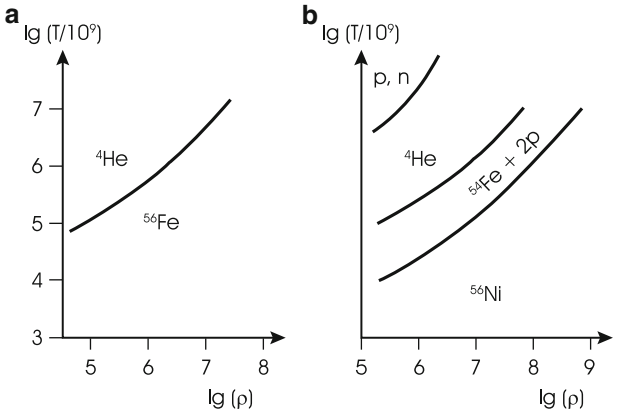

Fig. 36.3 (**a**) In the temperature-density diagram (T in 10^9 K, ϱ in g cm^{-3}) the curve separates the regions in which equilibrium demands matter to be in the form of ^{4}He and ^{56}Fe, respectively, for the case of $\bar{Z}/\bar{N} = 13/15$. (**b**) The corresponding equilibrium regions for $\bar{Z}/\bar{N} = 1$

36.2.3 Hydrostatic and Convective Adjustment

Even during the rapid helium flash the star remains very nearly in hydrostatic equilibrium, and convection can carry away all the released nuclear energy without becoming appreciably superadiabatic. The situation is completely different if unstable carbon burning proceeds in a degenerate core on a time-scale of milliseconds.

Consider the events after the onset of the carbon flash in the centre. The rapid rise of the central temperature is sufficient for immediately starting higher nuclear reactions, such as oxygen burning, which release additional energy. In one single runaway the central temperature rises so much that statistical equilibrium between Fe and He is reached, and eventually degeneracy is removed (see Fig. 36.2). Then the pressure increases and the central region starts to expand. This will occur roughly on a timescale τ_ε, in which the central temperature and the internal energy u rise. Since $\dot{T}/T \approx \varepsilon_{\rm CC}/u$, we have

$$\tau_\varepsilon = \frac{c_P T}{\varepsilon_{\rm CC}}. \tag{36.20}$$

The other regions of the core react on the central expansion on the hydrostatic timescale $\tau_{\rm hydr} \approx (G\bar{\varrho})^{-1/2}$ [compare with (2.19)], where $\bar{\varrho}$ is the mean density of the core. As long as $\zeta := \tau_\varepsilon/\tau_{\rm hydr} \gg 1$ the core follows the central expansion quasi-hydrostatically. If, however, $\zeta \ll 1$, then the layers above cannot react rapidly enough, and a compression wave will move outwards with the speed of sound. If the push by the suddenly expanding burning region is sufficiently strong, an outwards travelling shock wave may develop.

Owing to the energy release in the flash, a central convective core will form, which has two effects. Part of the surplus energy is carried away (reducing the

intensity of the flash), and new nuclear fuel is brought to the region of carbon burning (enhancing the flash). A characteristic timescale for convection is $\tau_{\rm conv} \approx \ell_{\rm m}/v_{\rm s}$, where $\ell_{\rm m}$ is the mixing length and $v_{\rm s}$ the local velocity of sound. Indeed turbulent elements will scarcely move faster than $v_{\rm s}$, since otherwise shock waves would strongly damp the motion. If $\xi := \tau_\varepsilon/\tau_{\rm conv} \gg 1$, convection is able to carry away all the nuclear energy released. If, however, $\xi \ll 1$, then convection cannot carry away the released energy.

The timescales $\tau_{\rm hydr}$ and $\tau_{\rm conv}$ are very short indeed. For the central parts of the core with $\varrho > 10^8\,{\rm g\,cm^{-3}}$, one finds typically $\tau_{\rm hydr} \approx 0.1\,{\rm s}$, and $\tau_{\rm conv}$ is of the same order. However, for $T = 2 \ldots 3 \times 10^9\,{\rm K}$, the local timescale τ_ε for the flash is of the order of $10^{-6}\,{\rm s}$. Therefore ζ and ξ are both $\ll 1$. This means that, instead of hydrostatic adjustment, a compression wave will start outwards and that "convective blocking" prevents a rapid spread of released energy in the core. The changes caused by the flash in one mass element propagate comparatively slowly to other parts.

These estimates clearly show that the carbon flash and the following explosion can be treated accurately only when the full hydrodynamical equations are solved. The important role of convection and the propagation of burning fronts necessitate three-dimensional models. Such models are the current state of the art, but will not be the subject of this book.

36.2.4 Combustion Fronts

The local nuclear timescale τ_ε at the onset of the flash is rather short. If a flash is started somewhere in a degenerate CO-core, the burning proceeds at such high rates that the fuel in this mass element is used up almost instantaneously. To be more precise, the consumption is completed locally before the layers above can adjust. Only then is the unburnt material ahead heated to ignition (either by compression or by energy transport, which may be by convection), and the flash proceeds outwards. But the burning is always confined to a layer of (practically) zero thickness. We have an outward-moving *combustion front*, which can be of two different types.

We have seen that a shock wave develops. Matter in front penetrates the discontinuity with supersonic velocity and is compressed and heated. If this suffices to ignite the fuel, then the combustion front coincides with the shock front moving outwards supersonically. This is called a *detonation front.* It releases enough energy to lead to a complete stellar explosion, but matter ahead of the blast wave cannot expand and ignites under typical white-dwarf conditions. Temperatures and densities are so high that NSE is reached and is peaking around Ni. This is in conflict with the presence of intermediate-mass elements seen in the spectra of some type Ia supernovae.

If the compression in the shock does not ignite the fuel, then the ignition temperature is reached owing to energy transport (convection or conduction). This gives a slower, subsonic motion for the burning front and contains a discontinuity in which density and pressure drop. This is a *deflagration front.* Since it allows the

nucleosynthesis to occur at lower density and pressure, NSE peaks at lower mass numbers and intermediate-mass elements can be created. Whether such deflagration models can unbind completely the white dwarf is unclear. Higher-dimensional simulations seem to be more promising to achieve this.

Obviously the speed of a deflagration front is controlled by that of energy transport. This in turn depends on the conductivity (thermal or convective) and on the temperature difference between the deflagration front and the material ahead. Numerical modelling thus needs hydrodynamical simulations of convection. Simple mixing length theory (Chap. 7), which has been useful for hydrostatic stellar evolution phases, certainly will not suffice to compute accurate models.

In both cases the deviations from hydrostatic equilibrium are mainly confined to a thin shell across which the pressure is discontinuous and all nuclear energy is released. The momentum of the matter approaching a detonation front supersonically is balanced by the higher pressure behind the front; the momentum of the matter approaching a deflagration front subsonically is balanced by the recoil of the matter moving away from it behind the front. The front in both cases is unstable to spatial perturbations, the scale of which is well below any numerical resolution in the simulations, and must be represented by a physical subscale model.

For an account of the theory of the two types of combustion fronts, see Courant and Friedrichs (1976), Landau and Lifshitz (1987), and Hillebrandt and Niemeyer (2000). As with normal shock waves, the theoretical results follow from the conservation of mass, momentum, and energy of the matter going through the discontinuity. For energy conservation, however, it also has to be taken into account that energy is released at the discontinuity. This makes the *two* types of solutions (detonation and deflagration waves) possible, while the theory of normal shock waves allows only that solution in which the density of matter going through the discontinuity increases.

In principle, detonation fronts as well as deflagration fronts can occur in stars. Which of the two will develop depends on the details of the transport mechanism, which determines the motion of a deflagration front and of the preceding shock.

In some cases the explosion may start out with a slow deflagration front, which allows some expansion of the layers ahead of the front, but which switches at some point into a detonation, when the front begins to progress supersonically. These are the *delayed detonation models*, which combine the advantage of allowing intermediate-mass elements to be created and deliver typical supernova energies, which are of order 10^{51} erg.

The details of type Ia supernova explosions can be uncovered only by very complicated and challenging numerical simulations that take into account both hydrodynamics and nuclear processes, and should resolve scales ranging from that of white dwarfs ($\sim 1,000$ km) down to that of the burning flame of a few cm. Early one-dimensional hydrodynamical calculations for detonation models were done by Arnett (1969) and Ivanova et al. (1977). A classical deflagration model, still in one dimension, is by Nomoto et al. (1976) and Nomoto (1984). State-of-the-art models are mostly 3-dimensional; a summary and discussion can be found in the reviews by Hillebrandt and Niemeyer (2000) and Roepke (2008).

36.2.5 Carbon Burning in Accreting White Dwarfs

Rather similar phenomena to those described above for CO-cores of single stars can occur in CO white dwarfs which are members of binary systems. They can receive appreciable amounts of matter from their companions. The accreted matter is compressed and heated, and its ignition can give rise to various phenomena.

For example, if helium is accreted with relatively low rates (about $10^{-8} M_\odot$/ year), a helium flash will be ignited in a shell of high density. The result can be a double detonation wave: a helium detonation front running outwards and a carbon detonation front going to the centre. As a result the white dwarf will be disrupted.

For higher accretion rates the new material can burn quietly near the surface, thus simply increasing the mass of the CO white dwarf. When it approaches $M_{\rm Ch}$, the density in the inner parts becomes so large that carbon burning starts either in the centre, or in the shell of maximum temperature. This results in a flash, and a deflagration (or detonation) front starts, as discussed above for single stars. The white dwarf will also be disrupted. Both possibilities correspond to Case 1 of Sect. 36.1. It is this mechanism which is generally believed to cause the Type Ia supernovae. Note that it has to be invoked, since the spectra of these supernovae show no hydrogen, and because evolving single stars of $M < 10 M_\odot$ may lose so much mass that their CO-core can never come close to $M_{\rm Ch}$.

36.3 Collapse of Cores of Massive Stars

According to Fig. 36.1 one can expect that the cores of massive stars will not cool, because of non-relativistic degeneracy, but will heat up during core contraction until the next type of nuclear fuel is ignited. The core then is either non-degenerate (larger core mass $M_{\rm c}$) or degenerate but to the upper right of the "summit" of the line $\alpha = 3/4$ in Fig. 28.1. In both cases the gravothermal heat capacity is negative, and the burning is self-controlled. In the following we discuss stars with core masses in the range $M_{\rm ch} < M_{\rm c} < 40 M_\odot$. The evolutionary paths of these stars will avoid the region of $\alpha < 3/4$, where in Fig. 28.1 the arrows point downwards.

After going through several cycles of nuclear burning and contraction, the core will heat up to silicon burning. Nuclear burning in several shell sources has produced layers of different chemical composition, as shown in Fig. 36.4. Finally the central region of the core reaches a temperature at which the abundances are determined by nuclear statistical equilibrium. In this stage the core is in a peculiar state in several respects. Since the electron gas dominates the pressure, and since at temperatures of $T_9 \approx 10$ the electrons are relativistic ($kT \approx 1.7 m_{\rm e} c^2$), the adiabatic exponent $\gamma_{\rm ad}$ is close to 4/3. In the more massive stars photodisintegration of heavy nuclei reduces $\gamma_{\rm ad}$ even more (like partial ionization). In addition general relativistic effects increase the critical value of $\gamma_{\rm ad}$ above 4/3, and the core becomes dynamically unstable. As a consequence core collapse sets in. For less massive stars the relativistic electrons are degenerate with high Fermi energies. Then electron

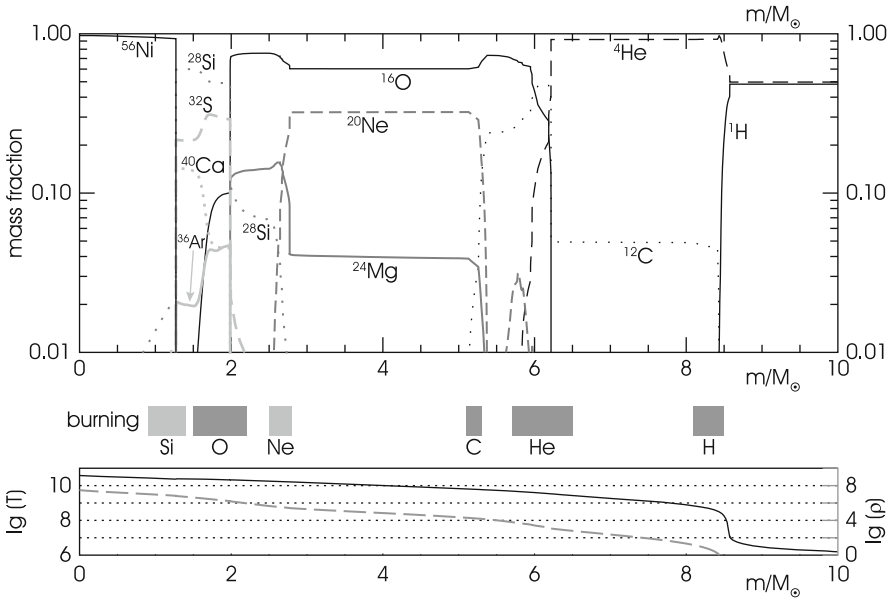

Fig. 36.4 The chemical composition in the interior of a highly evolved model of a population I star with an initial mass of $25M_{\odot}$, close to the end of hydrostatic nuclear burning. The mass at this time is reduced to $16M_{\odot}$ due to mass loss. In the *upper panel* the mass concentrations of important elements are plotted against the mass variable m. *Below* the abscissa, in the *middle* of the figure, the approximate location of shell sources in different nuclear burning phases is indicated by the *grey rectangles*. In the *lower panel* the run of temperature ($\lg T$: scale at *left axis*) and density ($\lg \varrho$: *right axis*) is given to identify typical burning conditions for these nuclear shells (data courtesy R. Hirschi, published in Hirschi et al. 2004)

captures by heavy nuclei reduce the pressure and start the collapse. For this stage we now discuss a simple solution.

36.3.1 Simple Collapse Solutions

Suppose we have a core at the onset of collapse, say, with central values $\varrho_0 = 10^{10}\,\mathrm{g\,cm^{-3}}, T_0 \approx 10^{10}\,\mathrm{K}$. The electrons are relativistically degenerate. Then the equation of state is polytropic and can be written as

$$P = K'\varrho^{4/3}, \tag{36.21}$$

where $K' = K_{4/3}/\mu_{\mathrm{e}}^{4/3}$ [compare with (15.26)]. Therefore the core can be described by a polytrope of index 3. We have already discussed the collapse of such a polytrope in Sect. 19.11. As we have seen there, the parameter λ appearing in the modified Emden equation (19.81) is a measure of the deviation from hydrostatic

equilibrium, which corresponds to the value $\lambda = 0$. Solutions with finite radius are possible only for values $0 < \lambda < \lambda_m = 6.544 \times 10^{-3}$, where $\lambda = \lambda_m$ corresponds to the strongest deviation from equilibrium. For $\lambda = \lambda_m$ no homologous collapse of a polytrope of $n = 3$ is possible.

We now adapt the formalism of Sect. 19.11 for application to the collapse of stellar cores. The solution of the spatial structure is given by the function $w(z)$, which obeys (19.81). We denote the value of z at the surface of the collapsing core by z_3, so that $w(z_3) = 0$; for $\lambda = 0$ one has $z_3 = 6.897$. It increases with λ and reaches the maximum value 9.889 for $\lambda = \lambda_m$. The limit $\lambda = \lambda_m$ is reached when the surface of the core collapses with the acceleration of free fall.

If we apply (19.75) to the surface we have

$$z_3 \ddot{a} = -\frac{4}{3}\lambda \frac{(K')^{3/2}}{\sqrt{\pi G}} \frac{z_3}{a^2}. \tag{36.22}$$

If this is equal to the free-fall acceleration $-GM_c/(az_3)^2$, then

$$\lambda = \lambda_m = \frac{3}{4}\sqrt{\frac{\pi G}{K'^3}} \frac{GM_c}{z_3^3}. \tag{36.23}$$

On the other hand, (19.67) and (19.81) give

$$\frac{\varrho}{\varrho_0} = w^3 = \lambda - \frac{1}{z^2}\frac{d}{dz}\left(z^2 \frac{dw}{dz}\right), \tag{36.24}$$

and therefore with $r = az$, $R_c = az_3$, and

$$\bar{\varrho} = \frac{3}{R_c^3}\int_0^{R_c} \varrho r^2 dr, \tag{36.25}$$

after some manipulation we find

$$\frac{\bar{\varrho}}{\varrho_0} = \lambda - \left[\frac{3}{z}\left(\frac{dw}{dz}\right)\right]_{z=z_3}. \tag{36.26}$$

If we apply this to the limit case $\lambda = \lambda_m$ in which dw/dz vanishes at the surface (compare with Fig. 19.3), we find $\bar{\varrho}/\varrho_0 = \lambda_m$.

The core may start out from the (marginally stable) equilibrium for which $\lambda = 0$. Here the actual acceleration at the surface is zero, since gravity and pressure gradient cancel each other. But if the pressure is slightly decreased, the core will start to collapse ($\lambda > 0$). The numerical integration of (19.81) for different values of λ in the range $0 \le \lambda \le \lambda_m$ gives values for z_3 and $\bar{\varrho}/\varrho_0$ in the ranges $6.897 \le z_3 \le 9.889$ and $0.01846 \le \bar{\varrho}/\varrho_c \le 0.0654$ (Goldreich and Weber 1980). If we determine the masses for different collapsing polytropes, we can use the expression

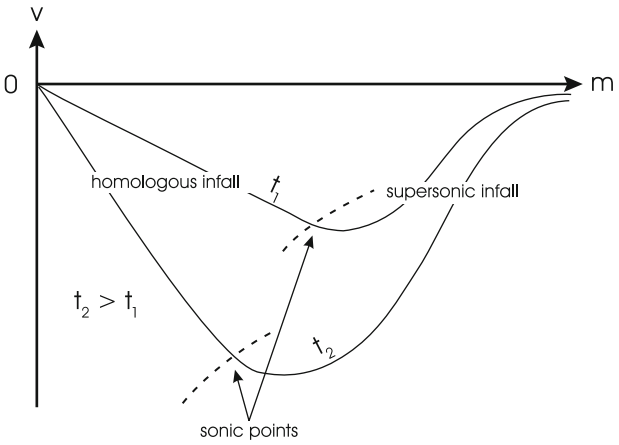

Fig. 36.5 Schematic picture of the velocity distribution in a collapsing stellar core obtained in numerical calculations, and taken at two subsequent times t_1 and t_2. Note the two regimes: on the *left* $|v_r|$ increases in the outward direction. It corresponds to a (roughly) homologously collapsing part, while on the *right* $|v_r|$ decreases with m. This corresponds to the free-fall regime, where velocities are supersonic. The run of the (negative) sound speed is indicated by the *dashed lines*, and the location, where the infall becomes supersonic, by *arrows*. With time the mass of the "inner core" (defined as the part left of the maximum infall velocity) is decreasing. Velocities are of the order of $10^9\,\mathrm{cm\,s^{-1}}$ (after Müller 1997)

$$M_c \equiv \frac{4\pi a^3 z_3^3 \varrho_0}{3}\frac{\bar{\varrho}}{\varrho_0} = \frac{4\pi z_3^3}{3}\left(\frac{K'}{\pi G}\right)^{3/2}\frac{\bar{\varrho}}{\varrho_0}, \tag{36.27}$$

which has been derived with the help of (19.67). Equation (36.27) for $\lambda = 0$ gives the Chandrasekhar mass M_{Ch}, as can be seen from (19.29), (19.30) and (36.26). In fact all masses obtained for different values of λ in the narrow interval $0 \le \lambda \le \lambda_m$ are close to the Chandrasekhar mass, namely $M_{\mathrm{Ch}} \le M_c \le 1.0499 M_{\mathrm{Ch}}$.

Only core masses in this small interval can collapse homologously. Now we know that $M_{\mathrm{Ch}} \sim \mu_e^{-2}$. Electron captures during the collapse increase μ_e and reduce M_{Ch}. Therefore the upper bound for M_c for homologous collapse decreases. If initially $\mu_e = \mu_{e0}$ and $M_{\mathrm{Ch}} = M_{\mathrm{Ch0}}$, then after some time not more than the mass

$$M_c = 1.0499\left(\frac{\mu_{e0}}{\mu_e}\right)^2 M_{\mathrm{Ch0}} \sim \mu_e^{-2} \tag{36.28}$$

can collapse homologously (Note that, strictly speaking, the whole formalism should be repeated for a time-dependent K'.). Numerical integrations in fact indicate that during collapse the mass of the homologously collapsing part of the core decreases with increasing μ_e as given by (36.28).

This simple collapse model has been generalized by Yahil and Lattimer (1982) for values of the polytropic index in (36.21) between $6/5 < \gamma_{\mathrm{ad}} < 4/3$. Figure 36.5 shows the infall velocity as a function of m as obtained from numerical

computations, in agreement with the models by Goldreich and Weber, and Yahil and Lattimer. The maximum separates the homologously collapsing inner core (left) from the nearly free-falling outer part of the core (right). The outer core collapses supersonically; the sound speed is exceeded at a location somewhat interior to the maximum collapse velocity. During collapse the boundary between the two regimes is not fixed but moves to smaller m values: mass from the inner core is released into the free-fall regime. This corresponds to the decrease of M_{Ch} with increasing μ_{e} as discussed above.

The collapse is extremely short-lived; it takes a time which is of the order of the free-fall time. If the core starts with an initial density of $10^{10}\,\mathrm{g\,cm^{-3}}$ one obtains $\tau_{\mathrm{ff}} \approx (G\bar{\varrho})^{-1/2} \approx 40$ ms at the onset of collapse, while it is 0.4 ms for $\bar{\varrho} = 10^{14}\,\mathrm{g\,cm^{-3}}$.

36.3.2 The Reflection of the Infall

Because of the collapse, the density finally approaches that of neutron stars (nuclear densities of the order $10^{14}\,\mathrm{g\,cm^{-3}}$). Then the equation of state becomes "stiff," i.e. the matter becomes almost incompressible. This terminates the collapse.

If the whole process were completely elastic, then the kinetic energy of the collapsing matter would be sufficient to bring it back after reflection to the state just before the collapse began. This energy can be estimated roughly from

$$E \approx GM_{\mathrm{c}}^2 \left(\frac{1}{R_{\mathrm{n}}} - \frac{1}{R_{\mathrm{wd}}} \right) \approx \frac{GM_{\mathrm{c}}^2}{R_{\mathrm{n}}} \approx 3 \times 10^{53}\mathrm{erg}, \tag{36.29}$$

where M_{c} is the mass of the collapsing core, while R_{n} and R_{wd} are the typical radii of a neutron star and of a white dwarf. We compare this with the energy E_{e} necessary to expel the envelope, which had no time to follow the core collapse,

$$E_{\mathrm{e}} = \int_{M_{\mathrm{wd}}}^{M} \frac{Gm\,dm}{r} \ll \frac{GM^2}{R_{\mathrm{wd}}} \approx 3 \times 10^{52}\mathrm{erg} \tag{36.30}$$

for $M = 10M_{\odot}$. Realistic estimates bring E_{e} down to 10^{50} erg, and therefore only a small fraction of the energy involved in the collapse of the core is sufficient to blow away the envelope. In predicting what happens after the bounce, one has to find out what (small) fraction of the energy of the collapse can be transformed into kinetic energy of outward motion. Remember that the energy estimated in (36.29) would suffice only to bring back the whole collapse to its original position–and no energy would be left for expelling the envelope. But if a remnant (neutron star) of mass M_{n} remains in the condensed state, the energy of its collapse is available. The question is how this can be used for accelerating the rest of the material outwards.

A possible mechanism would be a shock wave moving outwards. The remnant is somewhat compressed by inertia beyond its equilibrium state and afterwards,

acting like a spring, it expands, pushing back the infalling matter above. This creates a pressure wave, steepening when it travels into regions of lower density. The kinetic energy stored in such a wave may be sufficient to lift the envelope into space. However, the following problem arises. One can imagine that the neutron star formed has a mass of the order of the final Chandrasekhar mass M_{ChF}. The rest of the collapsing matter still consists mainly of iron. When, after rebounce, this region is passed by the shock wave, almost all of its energy is used up to disintegrate the iron into free nucleons. Therefore only a small fraction of the initial kinetic energy remains in the shock wave and is available for lifting the envelope.

In fact the major part of the energy estimated in (36.29) of order 10^{53} erg is lost in the form of neutrinos (Sect. 36.3.3). Only 1 % of it–10^{51} erg–is actually converted into kinetic energy, and only a few per cent of this is escaping from the supernova in the form of light. Nevertheless, this tiny part of the collapse energy makes supernovae the brightest stellar objects in the universe.

36.3.3 Effects of Neutrinos

Before collapse, neutrinos were created by the processes described in Sect. 18.7, and their energy is of the order of the thermal energy of the electrons. During collapse, neutrino production by neutronization becomes dominant. As soon as the density approaches values of $10^{12}\,\mathrm{g\,cm^{-3}}$, inverse β decay becomes more pronounced, and the equilibrium shifts to increasingly neutron-rich nuclei. During this neutronization neutrinos are released. In connection with supernova SN 1987A, neutrinos have been observed in underground neutrino detectors–manifest evidence that core collapse is indeed connected with the supernova phenomenon. The typical energy of the neutrinos released during collapse is of the order of the Fermi energy of the (relativistic) electrons. Therefore when using the relation $\varrho = \mu_{\mathrm{e}} n_{\mathrm{e}} m_u$ and (15.11) and (15.15) one finds

$$\begin{aligned}\frac{E_\nu}{m_{\mathrm{e}}c^2} &\approx \frac{E_{\mathrm{F}}}{m_{\mathrm{e}}c^2} = \frac{p_{\mathrm{F}}}{m_{\mathrm{e}}c} \\ &= \left(\frac{3}{8\pi m_{\mathrm{u}}}\right)^{1/3} \frac{h}{m_{\mathrm{e}}c} \left(\frac{\varrho}{\mu_{\mathrm{e}}}\right)^{1/3} \approx 10^{-2} \left(\frac{\varrho}{\mu_{\mathrm{e}}}\right)^{1/3}. \end{aligned} \tag{36.31}$$

If heavy nuclei are present, the neutrinos interact predominantly through the so-called "coherent" scattering (rather than scattering by free nucleons):

$$\nu + (Z, A) \rightarrow \nu + (Z, A). \tag{36.32}$$

The cross section is of the order of

$$\sigma_\nu \approx \left(\frac{E_\nu}{m_{\mathrm{e}}c^2}\right)^2 A^2 10^{-45}\mathrm{cm}^2, \tag{36.33}$$

which with (36.31) gives

$$\sigma_\nu \approx A^2 \left(\frac{\varrho}{\mu_\mathrm{e}}\right)^{2/3} 10^{-49}\mathrm{cm}^2. \tag{36.34}$$

This allows an estimate of the mean-free-path ℓ_ν of neutrinos in the collapsing core. If $n = \varrho/(Am_\mathrm{u})$ is the number density of nuclei, then with (36.34)

$$\ell_\nu \approx \frac{1}{n\sigma_\nu} = \frac{1}{\mu_\mathrm{e} A}\left(\frac{\varrho}{\mu_\mathrm{e}}\right)^{-5/3} 1.7 \times 10^{25}\mathrm{cm}. \tag{36.35}$$

Can ℓ_ν become comparable with the dimension of the collapsing core, say, 10^7 cm? With $\mu_\mathrm{e} = 2, A \approx 100$, we obtain from (36.35) $\ell_\nu = 10^7$ cm for $(\varrho/\mu_\mathrm{e}) = 3.6 \times 10^9\,\mathrm{g\,cm^{-3}}$. We may bring (36.35) into a more convenient form by putting in such typical values for μ_e, A, and ϱ such that it yields a typical length

$$\ell_\nu \approx \frac{1}{n\sigma_\nu} = \frac{200}{\mu_\mathrm{e} A}\left(\frac{2\varrho}{10^{10}\mu_\mathrm{e}}\right)^{-5/3} 5.8 \times 10^6\ \mathrm{cm}. \tag{36.36}$$

Obviously we cannot simply assume that the neutrinos escape without interaction. The more the density rises, the smaller ℓ_ν, and the collapsing core becomes opaque for neutrinos. Then they can only diffuse through the matter via many scattering processes. For sufficiently high density the diffusion velocity becomes even smaller than the velocity of the collapse. Calculations show that the neutrinos cannot escape by diffusion within the free-fall time τ_ff of the core if $\varrho \gtrsim 3 \times 10^{11}\,\mathrm{g\,cm^{-3}}$: the neutrinos are then trapped.

In the schematic picture of the core structure (Fig. 36.6), the place where the infall velocity of matter equals the velocity of outward neutrino diffusion is indicated as the "neutrino trapping surface". Below it the neutrinos are trapped; above it they diffuse outwards until reaching the so-called "neutrinosphere". This provides the boundary of the opaque part of the core and is located one mean free path ℓ_ν beneath the surface. From here the neutrinos leave the core almost without further interaction.

Detailed calculations have to deal with a radiation-hydro-problem, where one has to solve the neutrino transport problem in a six-dimensional phase space, defined by three spatial and three momentum coordinates, one of the latter being the neutrino energy, for example. In particular one has to consider and calculate the detailed distribution function of the neutrinos (rather than their average energy). This is obvious since the cross section as given in (36.33) depends on the energy of the neutrinos: those with low energy can escape more easily than those of high energy. This problem, which is essentially that of solving the Boltzmann equation, requires very extensive and challenging computations and has not been solved so far in all aspects for realistic physical conditions. Another important aspect is the detailed consideration of all neutrino interactions with matter, including neutrino oscillations and cross sections for the different neutrino families. The neutrino transport is essential for modelling type II supernova explosions as the neutrinos deposit part of

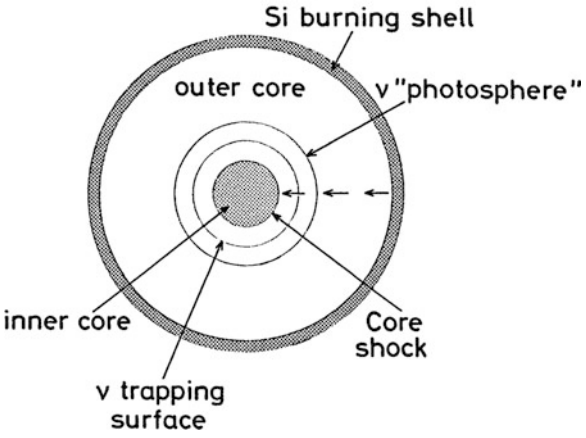

Fig. 36.6 Schematic picture of a collapsing stellar core at bounce. The *short arrows* correspond to the velocity field. At the sphere labelled *core shock,* the shock is formed. Inside this sphere the *matter* is almost at rest. Above the shock there is a still collapsing shell in which neutrinos are trapped. But on top there is a shell from which neutrinos can escape. One can define a neutrino photosphere, a *neutrinosphere*, analogous to the photosphere in a stellar atmosphere

their energy below the neutrinosphere, possibly raising the energy to levels sufficient to expel the envelope.

The congestion of the neutrinos, resulting from the opaqueness of the core, influences the further neutronization. With increasing density the neutrinos become degenerate with a high Fermi energy. Electron capture becomes less probable, since the new neutrinos have to be raised to the top of the Fermi sea. Around a density of $3\times10^{12}\,\mathrm{g\,cm^{-3}}$ the so-called β-equilibrium is reached, where the reaction $p+e^- \leftrightarrow n+\nu_e$ proceeds in both directions. However, the neutrino capture reaction is also subject to the requirement that the resulting electron has to have an energy above the Fermi energy of the degenerate electron gas. In total, with increasing density, β-equilibrium shifts to the right-hand side. Since the neutrinos can no longer escape, the number of leptons (electrons and neutrinos) stays constant. γ_{ad} has increased to a value close to $4/3$, which corresponds to relativistic degeneracy. The collapse continues until $\varrho > 10^{14}\,\mathrm{g\,cm^{-3}}$, the nuclear density. At such densities the equation of state is very stiff, and $\gamma_{\mathrm{ad}} \gtrsim 2$ due to the repulsive nuclear forces of the strong interaction. Therefore the collapse is stopped. Further neutronization can proceed only as far as the neutrinos diffuse outwards. This enables further electron captures on protons, lowering the proton-to-neutron ratio. Most of this takes place in the neutronization shell between trapping surface and neutrino photosphere (Fig. 36.6) where the density is several $10^{11}\,\mathrm{g\,cm^{-3}}$. During this phase, which can last a few to 10 s, the proto-neutron star evolves into a neutron star.

As in the case of thermonuclear supernova explosions caused by the carbon flash detailed models are possible only by two- and three-dimensional hydrodynamical simulations, taking into account nucleosynthesis and the problem of neutrino

transport in full detail. Another major ingredient is the equation of state at nuclear matter density, finite temperature, and for extremely neutron-rich matter. Such computations are extremely demanding, require always the latest generation of supercomputers, but are still from giving final answers concerning the details of core collapse supernova explosions. Some of these simulations have resulted in successfully exploding pre-SN models, other have failed or remained inconclusive. We therefore refer the reader to some recent reviews about the subject, given by Woosley and Janka (2005), Mezzacappa (2005), and Janka et al. (2007).

36.3.4 Electron-Capture Supernovae

While electron capture plays an important role in all core-collapse supernovae, it is particularly crucial in the specific case of degenerate NeOMg cores reaching a critical density of $4.5 \times 10^9 \mathrm{g\,cm^{-3}}$, equivalent to a mass of $1.37 M_\odot$ (Nomoto et al. 1984). These conditions are reached, according to the models by Nomoto and others, within helium cores slightly less massive than $2.5 M_\odot$ in stars of an initial mass of about $9 M_\odot$ or somewhat higher, i.e. the super-AGB stars of Sect. 34.8 (see also Fig. 34.10).

The core collapse is initiated here by the capture of electrons on ^{24}Mg and ^{20}Ne, since this is energetically preferred over keeping the electrons at high energy in the Fermi distribution. This reduces pressure, which is mainly provided by the degenerate electrons, and contraction sets in. During the ensuing collapse oxygen burning starts, but the released nuclear energy is not sufficient to stop the collapse, since the energy budget is dominated by the loss due to neutrinos emitted in the electron-capture process. The nuclear burning proceeds to nuclear statistical equilibrium, which, in the course of the collapse, first shifts to α-particles and in the final phase to neutrons and protons. The result is a neutron star of low mass ($\lesssim 1.37 M_\odot$). According to numerical simulations (Kitaura et al. 2006) the supernova explosion is driven by the neutrino heating mechanism, and comparably small amounts of metals, in particular of O, C, and Ni ($< 0.015 M_\odot$), are ejected. The overall explosion energy is of order 10^{50} erg, and therefore much lower than in type II supernovae from more massive stars. These results agree with properties of the Crab supernova remnant and pulsar, and thus this historical supernova is believed to be of the electron-capture type. It could therefore be evidence for a previous super-AGB evolution. However, the absence of hydrogen in the Crab nebula points to a previous binary star evolution.

36.3.5 Pair-Creation Instability

From Fig. 36.1 one can see that evolutionary tracks for cores of sufficient mass enter a region on the left-hand side of the diagram where also $\gamma_{\mathrm{ad}} < 4/3$ (Fowler and Hoyle 1964). In this region many photons have an energy exceeding the rest-mass

energy of two electrons, $h\nu \geq 2m_e c^2$. Therefore electron-positron pairs can be spontaneously formed out of photons in the fields of nuclei. Admittedly the pairs do annihilate, creating photons again, but there is always an equilibrium number of pairs present. The *mean* energy of the photons $h\nu \approx kT$ equals the rest energy of the electron–positron pair only at a temperature of 1.2×10^{10} K, but even at 10^9 K appreciable pair creation occurs because of the high-energy photons of the Planck distribution.

For an account of the thermodynamic effects of pair creation, see, for example, Weiss et al. (2004). In many respects pair creation can be considered in analogy to ionization or dissociation (a photon being "ionized" or "dissociated" into a pair e^-, e^+). Regarding the stability of massive cores, the crucial point is that the pair creation reduces $\gamma_{\rm ad}$, as incomplete ionization or photodisintegration does. Indeed, if the gas is compressed, not all the energy is used to increase the temperature, but part of it is used to create pairs. Other reductions of $\gamma_{\rm ad}$ are due to high radiation pressure according to (13.7), (13.12) and (13.15) and to relativistic electrons. All these effects bring $\gamma_{\rm ad}$ below the critical value $4/3$ for dynamical instability.

The total number of electrons consists of those from pairs and those from normal ionization of atoms. With increasing ϱ the Fermi energy rises. This diminishes the possibility for pair creation, since newly created electrons now need an energy exceeding the Fermi energy. Correspondingly the instability region in Fig. 36.1 is limited to the right at a density of $5 \times 10^5\,\mathrm{g\,cm^{-3}}$.

The pairs created are not relativistic, having $\gamma_{\rm ad} = 5/3$ (Note that a photon with $h\nu = m_e c^2$ can only create a pair with zero kinetic energy!). For higher temperatures there are so many pairs that they dominate and bring $\gamma_{\rm ad}$ of the whole gas–radiation mixture slightly above $4/3$, which limits the instability region towards high temperatures. In summary, the three effects discussed in the preceding paragraphs explain the island nature of the pair-creation instability in Fig. 36.1.

For the evolution of cores into the region of pair instability, radiation pressure is important, and therefore one cannot use our simple formulae of Sect. 36.1. Furthermore, for a core instability, it is not sufficient that the evolutionary track of the star's *centre* moves through the area with $\gamma_{\rm ad} < 4/3$. Since in reality a mean value of $\gamma_{\rm ad}$ over the whole core decides upon its dynamical stability (Sect. 40.1), an appreciable fraction of the core mass must lie in that density–temperature range. According to numerical results this happens to cores of masses of $40M_{\rm crit}$ and more, where $M_{\rm crit}$ is defined in (36.5). The corresponding main-sequence masses depend on the uncertain mass loss, but a realistic guess seems to be that stars initially with $M > 80 - 100M_\odot$ later develop pair-unstable cores. This, however, assumes that no appreciable mass is lost due to radiation-driven stellar winds during the main-sequence phase. In addition, violent radial pulsations by the ϵ-mechanism (Sects. 41.1 and 41.5) may lead to a significant mass reduction for stars with $M \gtrsim 60M_\odot$. Both effects depend on metallicity. Therefore for solar metallicity models predict a maximum helium core mass of about $10M_\odot$, while for metal-free Pop. III stars, they may exceed the critical value for pair instability. It may be that this kind of supernova explosions may be restricted to the very early universe.

The final fate of stars this massive is rather uncertain. Numerical calculations indicate that, in a collapsing core of this type, oxygen is ignited explosively and the core runs into the (unstable) region of photodisintegration, which may cause a total disruption of the star. There is also the possibility of violent pulsations caused by the instability, which lead to explosive mass loss, but no total disruption. The star may thus (for increasing main-sequence mass) end in a black hole after having expelled large parts of its hydrogen/helium layers, be totally disrupted, or collapse directly into a black hole. The situation and the different outcomes have been summarized by Heger et al. (2003).

We also mention that rotation is playing a crucial role also for the final phases of massive star evolution, although the basic effects as discussed in this chapter remain the same. Details can be found in the textbook by Maeder (2009).

36.4 The Supernova-Gamma-Ray-Burst Connection

Gamma-ray bursts (GRBs) are short flashes of γ-radiation (energies in the range of 100 keV), which reach us from all directions in the sky and cosmological distances. They typically last for several ten seconds, but the total duration varies between fractions of a second to minutes. Repetitive events were never reported. The burst results from matter accelerated to highly relativistic speeds. The energy of this collimated matter jet is converted into radiation by an as yet not fully understood mechanism. The energy of the GRB is of the order of 10^{51} erg, which is the same order of magnitude as the kinetical energy of a core collapse supernova.

GRBs were detected in the 1970s by the military *Vela*-satellite, and most extensively investigated scientifically by the Batse detector on board of the *Compton Gamma Ray Observatory*. The event frequency is a few per day. While the shortest GRBs are thought to be the result of the merging of two neutron stars (or that of a neutron star with a black hole), the longer lasting type (longer than $\approx$ 2 s) has been associated with the core collapse of massive stars, mainly due to the association of GRBs with star-forming regions, and the coincidence, both in time and place, with SNe of type Ib and Ic. These are core collapse supernovae, which lack hydrogen in their spectra. For a review about this evidence, and more details about the connection, see Woosley and Bloom (2006).

Why do a few massive stars create highly collimated jets of matter, being ejected at more than 99.9 % of the speed of light, while the majority eject their envelopes more or less as a spherical shell? The answer is believed to lie in an exceptionally high rotation of the precursor's core. For very massive stars ($M > 30 M_\odot$), the core collapses into a fast-rotating black hole and infalling matter assembles in an accretion disk around it (the *collapsar* model). There are several mechanisms under discussion, how the binding energy of the disk or the rotation energy of the black hole can be converted into the collimated relativistic outflow. Alternatively, GRBs may originate from highly magnetized ($B \approx 1 \times 10^{15}$ G), fast-rotating neutron stars with rotation periods of milliseconds, thus rotating almost at breakup speed (the

magnetar model). The rotation energy would be of order 10^{52} erg, and the spin-down luminosity would be of the right order for a GRB.

The fact that hydrogen is absent in the spectra requires high mass loss rates as for Wolf-Rayet stars, but these should not be so high as to reduce the mass too much. Since mass loss scales somehow with metallicity, it is expected that GRBs should be found mainly in low-metallicity regions, and occur more frequently in the early epochs of the universe.

Although many details are still not understood, it seems to be evident that long-duration GRBs are core collapse supernovae with very massive progenitors that have extremely fast-rotating cores.